Characterizing Polymeric Methylene Diphenyl Diisocyanate Reactions with Wood: 2. Nano-Indentation

J.E. Jakes
Materials Science Program, University of Wisconsin-Madison;
U.S. Forest Products Laboratory, USDA Forest Service, Madison, Wisconsin

D.Y. Yelle
U.S. Forest Products Laboratory, USDA Forest Service, Madison, Wisconsin

J.F. Beecher
U.S. Forest Products Laboratory, USDA Forest Service, Madison, Wisconsin

C.R. Frihart
U.S. Forest Products Laboratory, USDA Forest Service, Madison, Wisconsin

D.S. Stone
Materials Science Program, University of Wisconsin-Madison;
Dep. of Materials Science and Engineering, University of Wisconsin-Madison

Abstract

In Part 1 of this study, two-dimensional solution-state nuclear magnetic resonance spectroscopy (2D solution NMR) found no covalent bonds between wood polymers and polymeric methylene diphenyl diisocyanate (pMDI) under the experimental conditions used. However, 2D solution NMR could not identify whether or not pMDI had entered the cell wall and if so, whether it polymerized in situ to create a polyurea interpenetrating polymer network (IPN). Here in Part 2, we employ recently developed nano-indentation techniques to assess the properties of cell walls in pMDI-infiltrated wood. The elastic modulus and hardness of the cell walls increased after pMDI modification, suggesting that pMDI infiltrated the cell walls to form a polyurea IPN inside the cell walls.

Introduction

Polymeric methylene diphenyl diisocyanate (pMDI) adhesives are known to produce durable bonds with wood substrates (Frazier 2003), but the mechanisms contributing to the durability are not wholly understood. Important aspects of bond durability include transferring stress across a bondline and accommodating swelling strains, such as when wood substrates swell in the presence of water. It has been proposed that pMDI adhesive durability is derived from components of the adhesive penetrating the wood structure and infiltrating the cell walls. The aim of this work is to further the understanding of the molecular-scale interaction between infiltrated pMDI and the polymeric constituents of wood. In Part 1 of this work (Yelle et al. 2009), two-dimensional solution-state nuclear magnetic resonance spectroscopy (2D solution NMR) was used to find that under the experimental conditions used, which were meant to mimic typical oriented strandboard bonding conditions, no covalent bonds between pMDI and wood polymers were found. Here in Part 2, we employ nano-indentation to measure the effects of pMDI on the mechanical properties of the wood cell wall. Even if pMDI does not form covalent bonds with the wood molecules, it is likely to alter the mechanical properties if it infiltrates into the cell wall. For instance, it might plasticize the cell wall polymers, or alternately, it might create an interpenetrating polymer network (IPN) that reinforces the cell walls.

Background

Potential Wood-pMDI Interactions

A molecular-scale schematic based on the work of Norimoto (2001) is used to aid in the discussion of

potential wood–pMDI interactions. The premise of the model (**Fig. 1**) is that the properties of the cell walls are largely influenced by hydrogen bonding among the three major cell wall polymers (cellulose, hemicelluloses, and lignin), and that chemicals infiltrated into the cell wall disrupt the hydrogen bonding or react to form additional covalent bonds. Difunctional components of pMDI could create covalent linkages between neighboring lignocellulosic chains (model B2) that would bulk and stiffen the cell wall. The derivatization of hydroxyl groups also decreases the hygroscopicity of the cell wall. Modifications of wood hygroscopicity would also contribute to changes in mechanical properties (Winandy and Rowell 2005). An isocyanate reacted with a single hydroxyl group (model B3) bulks the cell wall and depending on the chemistry of the newly attached molecule, may or may not affect the hygroscopicity of the cell wall. It is not clear how this type of molecular-scale interaction would affect cell wall mechanical properties. Infiltrated chemicals that do not form covalent bonds with the lignocellulosic chains (models B4 and B5) bulk the cell walls, and again, depending on the chemistry, may or may not affect the hygroscopicity. Small chemicals (model B4) would likely plasticize the cell wall, causing stiffness and strength to decrease. If a sufficient amount of chemicals infiltrated the cell wall and polymerized in situ, a reinforcing IPN (model B5) would form that may increase the stiffness and strength of the cell walls.

Isocyanate chemistry and previous work investigating the interactions between isocyanates and wood are discussed in Part 1 (Yelle et al. 2009). Potential isocyanate reactions include reactions with hydroxyl groups on wood polymers to form urethane linkages (model B2 or B3), reactions with water to form amines (model B4), followed by reaction of the newly formed amines and other isocyanates to form urea/biuret structures within the cell wall (model B4), or an IPN of polyurea within the cell wall (model B5). Identifying covalent bond formation between pMDI and wood is not trivial, but a 2D solution NMR technique capable of unambiguously detecting covalent bond formation between chemicals and the polymeric constituents of wood has recently been developed (Yelle 2009, Yelle et al. 2008). In Part 1, Yelle and coworkers (2009) used 2D solution NMR to seek out covalent bond formation between isocyanates and wood polymers reacted at different moisture contents and temperatures. The conclusion was that under typical bonding conditions, pMDI does not covalently bond with wood polymers, eliminating Norimoto models B2 and B3. However, the 2D solution NMR does not differentiate between possibilities B4 and B5. Here in Part 2, we will test Yelle and coworkers' specimens using nano-indentation. In addition to the pMDI-modified specimen, a specimen was also made by infiltrating the cell walls with monofunctional phenyl isocyanate (PI). A polyuret IPN is possible from PI, but is far less likely to form an IPN than the multifunctional pMDI. Therefore, the PI specimen is taken to represent model B4. We investigate whether it is possible to distinguish between the PI- (model B4) and pMDI- (model B4 or B5) modified wood using nano-indentation.

Nano-Indentation

Nano-indentation experiments consist of pressing an indenter, typically a diamond shaped as a three-sided pyramid, into a material while continuously recording the load and displacement. One attractive feature of nano-indentation is the small volume of material (usually between 10 nm to 10 µm across) that can be probed during the test. This makes nano-indentation a valuable tool to probe the properties of S2 cell wall laminae (S2CWL) and compound corner-middle lamellae (CCML) in wood. From nano-indentation data, the elastic modulus, hardness, and rate-dependent properties can be assessed. The pioneering work of Wimmer and coworkers on wood was completed more than a decade ago (Wimmer and Lucas 1997, Wimmer et al. 1997). Since that time, other researchers have used nano-indentation to probe the mechanical properties of different wood-adhesive bondlines (Gindl and Gupta 2002, Gindl et al. 2004a, 2004b, Konnerth and Gindl 2006, 2008, Konnerth et al. 2006), but to date no work has been reported on pMDI–wood interactions. Gindl and coworkers reported nano-indentation work on pMDI-modified wood (Gindl et al. 2004a), but in their erratum (Gindl et al. 2004b) they clarified that the pMDI was actually a one-component polyurethane.

We recently developed experimental nano-indentation methods to account for the non-idealities present in nano-indentation experiments performed on cell walls in wood. Most nano-indentation measurements on wood use the standard Oliver–Pharr (Oliver and Pharr 1992) nano-indentation analysis, disregarding that in wood the implicit assumption of the Oliver–Pharr analysis is being violated. This assumption is that the specimen is a homogeneous, rigidly supported half-space. Wood, in contrast, has much heterogeneity, such as the free edge between the cell wall lamina and lumen, which are in close proximity to the indent, and although the indents do not overlap the edge, the displacements upon which nano-indentation measurements rely are affected. In addition, wood is a cellular structure and during testing of cell-wall laminae, the entire specimen may flex, violating the rigid-support assumption. We recently discovered that the effects of both nearby heterogeneities and specimen-scale flexing could be simultaneously accounted for in nano-indentation measurements by incorporating a structural compliance, C_s, in the analysis (Jakes et al. 2008, Jakes et al. 2009). C_s behaves similarly to the machine compliance, C_m, and can be measured using methods similar to those used to determine C_m (Jakes et al. 2008). The C_m is independent of the size of the indent, has a positive value, and is a property of the instrument. C_s is also independent of the size of the indent, but it varies as a function of position within the specimen. We proposed assessing C_s in wood cell walls by determining the total unloading compliance, C_t, as a function of load from a multi-load indent and using

the modified Stone, Yoder, and Sproul (SYS) correlation (Stone et al. 1991) given by

$$C_t P_0^{1/2} = (C_m + C_s)P_0^{1/2} + J_0^{1/2} \quad [1]$$

where P_0 is the load immediately prior to unloading, and $J_0 = H/E^2_{eff}$ is the Joslin–Oliver parameter (Joslin and Oliver 1990) in which H is the Meyer hardness and E_{eff} is the "effective" modulus for contact. According to **Eq. [1]**, provided that there is no indentation size effect in the properties (i.e., J_0 is a constant), $C_t P_0^{1/2}$ plotted as a function of $P_0^{1/2}$ forms a straight line of slope $C_m + C_s$, and intercept $J_0^{1/2}$.

After the load-depth trace is corrected for the measured value of $C_m + C_s$, the unloading compliance attributable to the specimen and indenter (C_p) can be related to specimen and indenter properties using

$$C_p = \frac{1}{E_{eff} A_0^{1/2}} \quad [2]$$

where A_0 is the contact area. For indentation against a homogenous, isotropic, elastic half-space,

$$\frac{1}{E_{eff}} = \frac{1}{\beta}\left(\frac{1-\nu_s^2}{E_s} + \frac{1-\nu_d^2}{E_d}\right) \quad [3]$$

where E_s and E_d are Young's moduli and ν_s and ν_d are Poisson's ratios of specimen and indenter, respectively. β is a numerical factor set equal to 1.23 (Jakes et al. 2008).

In nano-indentation, the Meyer hardness (H) is typically calculated from the load and area immediately prior to unloading from

$$H = \frac{P_0}{A_0} \quad [4]$$

However, H is not a static property. Plastic deformation is thermally activated, and the flow-stress beneath the indenter depends on deformation rate. As a consequence of this, the value of H measured using **Eq. [4]** will depend on the rate of loading and length of the hold time prior to unloading. To capture the rate-dependent hardness, which potentially contains a wealth of information about the underlying structures and mechanisms controlling plasticity beneath the indenter, we have developed the broadband nano-indentation creep (BNC) technique. BNC is based on the creep analysis originally proposed by Stone and Yoder (1994) and recently improved and validated using finite element analysis (Elmustafa et al. 2007, Stone et al. 2010). During the hold segment of a force-controlled experiment, the instantaneous indentation depth, $h(t)$, increases and H decreases. The creep analysis calculates the H by first removing the elastic component of $h(t)$ to give the instantaneous plastic depth

$$h_p(t) \cong h_p^0 + \frac{h(t) - h_p^0 - P(t)C_p + P(t)C_p\left(1-\zeta_p\right)\dfrac{P(t)-P_0}{2P_0}}{1 - \dfrac{P(t)C_p}{h_p^0}\zeta_p} \quad [5]$$

where $P(t)$ is the instantaneous load during the creep segment, h_p^0 is the plastic depth at the end of the load segment ($h_p^0 = h_0 - C_p P_0$ where h_0 is depth at end of hold segment), and ζ_p is a power law exponent relating the instantaneous contact area, $A(t)$, and $h_p(t)$. The introduction of ζ_p into the creep analysis was guided by finite element analysis that showed the common assumption that contact area increases to the square of plastic depth for pyramid indenters breaks down, especially for materials with high hardness to elastic modulus ratios. Stone and coworkers therefore defined

$$\zeta_p = \partial \ln\sqrt{A} / \partial \ln h_p\Big|_{P_0} \quad [6]$$

to more accurately estimate $A(t)$ during the hold segment (Stone and Elmustafa 2008, Elmustafa et al. 2007). ζ_p can be determined experimentally (Puthoff et al. 2009). Instantaneous contact area is calculated using

$$A(t) \cong A_0\left(\frac{h_p(t)}{h_p^0}\right)^{2\zeta_p}, \quad [7]$$

and finally the instantaneous hardness

$$H(t) \cong \frac{P(t)}{A(t)} \quad [8]$$

To complete the analysis, a hardness strain rate, $\dot{\varepsilon}_H$, is defined as

$$\dot{\varepsilon}_H = \frac{d\ln\sqrt{A(t)}}{dt} \quad [9]$$

The BNC technique transforms nano-indentation from a tool that just measures mechanical properties, to a type of spectroscopic tool capable of identifying and understanding mechanisms controlling the plasticity operations beneath an indenter.

Materials and Methods

Specimens and Chemical Modifications

Latewood loblolly pine (*Pinus taeda* L.) matchstick-size (1 × 1 × 30 mm, with 30 mm dimension in the longitudinal direction) specimens cut from the same growth ring were modified with the five treatments in **Table 1**. These specimens were taken from the same batches used to prepare the specimens in the 2D solution NMR experiments in Part 1. The experimental details about the modifications

Table 1. ~ *Descriptions of tested specimens.*

Specimen ID†	Modifying species	M.C.‡	Temp.§	Covalent bonds formed?¶
		(%)	(°C)	
C	–	–	–	–
CH	–	14	160	–
PI14	PI	14	25	No
PI0H	PI	0	160	Yes
PI14H	PI	14	160	Yes
pMDI14H	pMDI	14	160	No

†Specimen IDs: "C" refers to control, "H" refers to heat applied during treatment, and "0" and "14" refer to the moisture content of the wood prior to treatment with phenyl isocyanate (PI) or pMDI.

‡Percentage of moisture content in the wood at the beginning of treatment.

§Temperature reaction was carried out at for 2 h.

¶Refers to covalent bond detected between isocyanates and wood polymers in Part 1 (Yelle et al. 2009).

are given in Part 1 (Yelle et al. 2009). Phenyl isocyanate was chosen because it is monofunctional and is less likely to form an IPN, while being similar in chemical reactivity to the pMDI. However, it can in principle react with a hydroxyl group in wood to form a urethane, or with water to form an amine, which can subsequently react with other isocyanate groups to form a urea or biuret molecule. These potential reactions correspond to B3 and B4 in the Norimoto schematic in **Fig. 1**. In Part 1, Yelle and coworkers (2009) showed that covalent bonds were detected in specimens PI0H (phenyl isocyanate reacted with nominally 0% moisture content wood at 160°C) and PI14H (phenyl isocyanate reacted with 14% moisture content wood at 160°C), but not PI14 (phenyl isocyanate reacted with 14% moisture content wood at room temperature). See **Table 1** for summary of treatments and nomenclature. We therefore believe that PI14 is model B4. The pMDI infiltrating into the cell wall could yield B2, B3, B4, or B5. Because no covalent bonds were found between pMDI and wood polymers in specimen pMDI14H in Part 1, B2 and B3 are eliminated from the potential molecular-scale interactions for these specimens. Nano-indentation results will be used in this work to try to distinguish between B4 and B5 in pMDI14H.

Wood surface preparation for nano-indentation is difficult. Previous researchers mostly embedded their specimens in epoxy (Gindl and Gupta 2002, Gindl et al. 2004a, 2004b, Konnerth and Gindl 2006, 2008, Konnerth et al. 2006, Wimmer and Lucas 1997, Wimmer et al. 1997). To eliminate the possibility of any undesired chemical modification caused by the epoxy, we developed a surface preparation procedure for unembedded wood (Jakes et al. 2008). The surface was prepared on the transverse plane. The procedure consists of carefully shaping a gently sloping (~15°) pyramid with disposable microtome blades in a sled microtome, then fitting the specimen in an ultra microtome with a diamond knife, and removing thin layers of material (<200 nm) from the apex of the pyramid until a suitably sized surface (~0.5 mm^2) is obtained. The specimen is fixed in the ultramicrotome so the cutting direction is parallel to the tangential direction in the wood. This orientation is found to consistently produce near artifact-free surfaces on the tangential side of trachieds, but irregular knife chatter marks more frequently form on the radial sides of trachieds and in the CCML. Chatter marks likely form more frequently in these regions because the cutting process is disrupted there as the knife-edge passes over the secondary cell wall and compound middle lamella interfaces. All of the cutting, both with the disposable blades and diamond knives, was done dry to limit further reactions of any unreacted isocyanates in the wood structure.

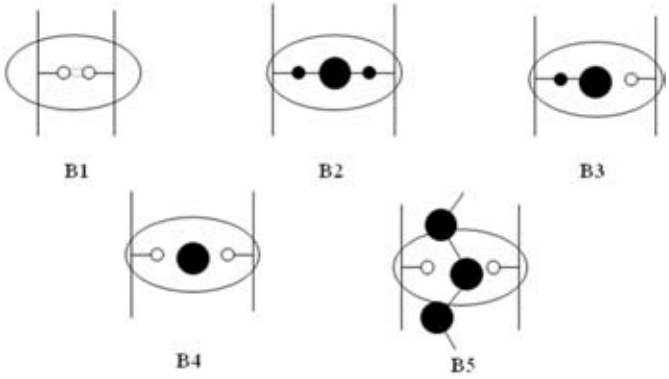

Figure 1. ~ *Potential models for the molecular-scale interactions between wood polymers and pMDI infiltrated into the cell wall on the basis of those originally proposed by Norimoto (2001). In these schematics, vertical lines represent lignocellulosic polymers, empty circles represent hydroxyl groups attached to the polymers, solid lines represent covalent bonds, dashed lines represent hydrogen bonds, small filled circles represent hydroxyl groups that were involved in the formation of covalent bonds, large filled circles represent infiltrated pMDI, and the increase in horizontal distance between the vertical lines represents swelling. Model B1 is the unmodified cell wall and potential molecular-scale wood–pMDI interactions are illustrated by models B2–5.*

Nano-Indentation

A Hysitron (Minneapolis, MN) Triboindenter equipped with a diamond Berkovich tip and operated in open-loop control was used in this work. Inside the nano-indentation enclosure, the relative humidity was maintained between 42 and 45% using a glycerin-water bath. The temperature was not locally controlled inside the enclosure and ranged between 22 and 28°C during these experiments. Specimens were placed inside the enclosure for a minimum of 48 h prior to experiments to allow equilibration. All indents in the S2CWL were placed on tangential side of the trachied. Only CCMLs formed by three trachieds, not four, were tested. For the indenter configuration used in this study, C_m was calculated using standard methods and found to be 2.8 μm/N.

A load-depth trace of an indent placed in the S2CWL of specimen C in **Table 1** is displayed in **Fig. 2**. The loading profile for BNC indents is designed for multiple

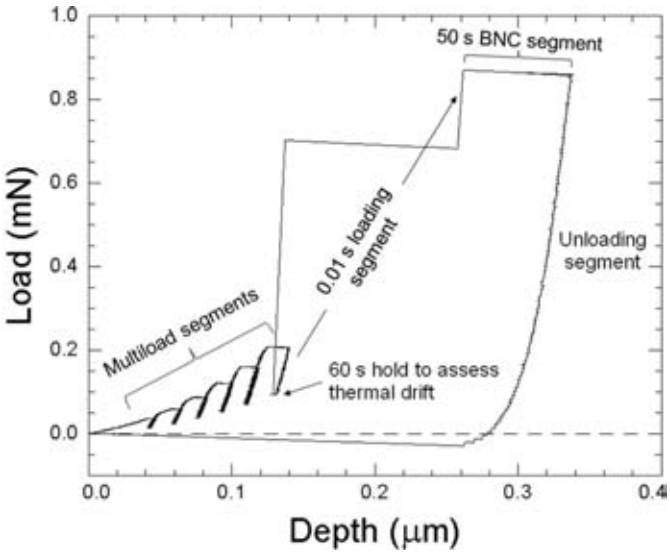

Figure 2. ~ *Load-depth trace of indent placed in S2CWL of specimen C.*

purposes. The first part of the load-depth trace consists of multi-load segments that provide the unloading compliance as a function of load to construct the SYS correlations used to assess structural compliances (Jakes et al. 2008, Jakes et al. 2009). The second portion is a 60-s hold during the final partial unload of the multi-load segments used to assess and correct the load-depth trace for thermal drift. Following the thermal drift segment, a 0.01-s loading segment leads to the 50-s BNC segment used in the analysis to assess hardness as a function of indentation strain rate. By trial and error in experiments performed on poly methylmethacrylate, we have found that the multi-load part needs to be 25% of maximum load to not affect the BNC segment. The large jog in the 0.01-s loading segment is a consequence of the finite loading capabilities of our nano-indenter and does not affect the BNC analysis. Finally, following the BNC segment the indenter is unloaded. After the load-depth has been corrected for thermal drift and $C_m + C_s$, the C_p is calculated as the inverse of the slope of the unloading segment immediately following the BNC segment. After assessing A_0, the elastic modulus is calculated using **Eqs.** [**2**] and [**3**]**,** and the BNC analysis is performed. On the basis of measurements from untreated wood, ζ_p was taken to equal 0.97 and 1.16 for the CCML and S2CWL, respectively.

The maximum loads for indents placed in S2CWL ranged from 0.7 to 1.0 mN, and the maximum load for all indents placed in CCML was 0.4 mN. Elastic moduli (E_s) of the materials in this study were calculated using **Eq.** [**3**], where E_d and ν_d for the diamond tip were assumed to be 1137 GPa and 0.07, respectively, and ν_s was 0.45 (Wimmer et al. 1997).

Atomic Force Microscopy

A Quesant (Agoura Hills, CA) atomic force microscope (AFM) incorporated in the Triboindenter was used to image all residual indents. The AFM was operated in contact mode and calibrated using an Advanced Surface Microscopy, Inc. (Indianapolis, IN) calibration standard with a pitch of 292 ± 0.5 nm. Successive scans and calibration routines reveal the reproducibility of the AFM calibration to be ±1%. ImageJ (http://rsb.info.nih.gov/ij/; verified 5 June 2010) image analysis software was used to manually measure the contact areas, A_0, used in the analyses from 4 µm field of view images. Overview AFM images of the cell walls are also used to observe changes in cellular structure caused by modifications.

Results and Discussion

Swelling of the S2CWL

AFM images of the prepared surfaces revealed a distinct region in the secondary cell wall layers that appeared only in the PI0H and PI14H specimens (**Fig. 3a**). In these specimens, the inner S2CWL, closest to the lumen, appeared to swell, pushing into the lumen. This region will be called the swollen S2CWL (sS2CWL). The dashed line in **Fig. 3a** highlights a portion of the distinct boundary between the sS2CWL and S2CWL that is distinguishable in the AFM image. The sS2CWL is thickest

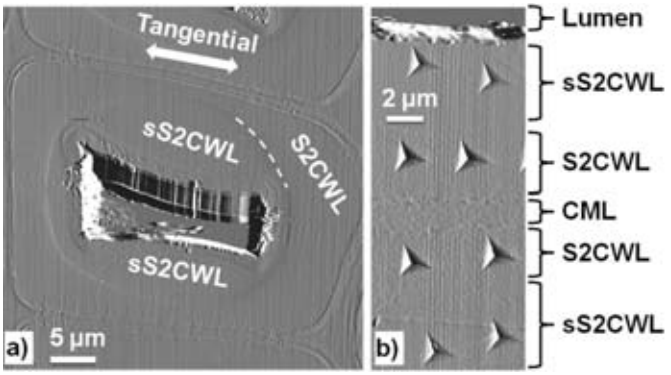

Figure 3. ~ *Atomic force microscope (AFM) images of a) surface prepared in specimen PI0H showing the sS2CWL and b) indents placed in the S2CWL and adjacent sS2CWL in specimen PI14H.*

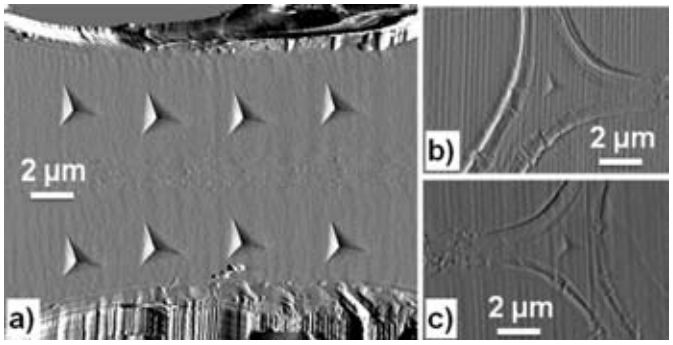

Figure 4. ~ *Atomic force microscope (AFM) images of indents placed in a) S2CWL of specimen CH, b) a CCML of PI14H, and c) a CCML of PI14.*

on the tangential side of the trachieds and thinnest at the corners. The sS2CWL was observed in all trachieds, but the proportions of the sS2CWL varied between trachieds. Therefore, we chose trachieds with approximately half the S2CWL swollen on the tangential side and placed indents in both the sS2CWL and S2CWL regions for the PI0H and PI14H specimens (**Fig. 3b**). The S2CWL for specimens C, CH, PI14, and pMDI14H appeared similar to the S2CWL in **Fig. 4a**. The CCML for all six specimens appeared similar to those in Fig. 4b and 4c.

Nano-Indentation Results

SYS correlations constructed from the multi-load segments for the indents placed in specimen PI0H are displayed in **Fig. 5**. The purpose of this plot is not to distinguish each SYS correlation, but to demonstrate that the SYS correlations separate into three distinct groups. The S2CWL data are closest to the bottom, CCML data are near the top, and sS2CWL data are in the middle. The intercepts of these correlations represent J_0 ($J_0 = H/E^2_{eff}$ from **Eq.** [**1**]) and the differences in J_0 for each group show that their properties differ. The values of $J_0^{1/2}$ and $C_m + C_s$ calculated from the SYS correlations are summarized in **Table 2** for all the specimens tested. The large variation between the average values of $C_m + C_s$ for the CCML is concerning and the large, positive values do not agree with our previous work that measured

$C_m + C_s \approx -2$ µm/N for indents placed in CCML (Jakes et al. 2009). A negative value of C_s is expected because the CCML is surrounded by the stiffer secondary cell wall laminae. The large uncertainty in the CCML SYS correlations in this work is probably caused by the surface roughness of the CCML surfaces. The multi-load indents used to construct the CCML SYS correlations were shallow, approximately 25 nm for the first partial unload and 100 nm for the final partial unload. The knife-chatter marks, vertical features in **Fig. 4b** and **4c**, prevented the construction of reliable SYS correlations for these shallow multi-loads. In our previous work, we indented similar CCMLs in loblolly pine using multi-load indents with maximum loads of 0.6 mN and partial unloads that spanned the entire load range. From these indents, we calculated $C_m + C_s \approx -2$ µm/N (Jakes et al. 2009). These results were more reliable than the current results and we therefore assumed a constant value of $C_m + C_s = -2$ µm/N in this work for the indents placed in the CCML. For the CCML, an uncertainty of 10 µm/N in C_s results in an uncertainty of 1 GPa for the elastic modulus, E_s, value. An uncertainty of 10 µm/N has less than a 1% effect on the hardnesses, H, in the BNC data.

The values of E_s for the S2CWL, sS2CWL, and CCML regions are displayed in **Fig. 6**. The S2CWL values for E_s range between about 15 and 20 GPa. The heat treatment did not have an effect on the S2CWL E_s. Specimen PI14 had a lower value of E_s and specimens PI14H and pMDI14H had higher values of E_s. The CCML values remained relatively constant and range between about 5.5 and 6.1 GPa. The E_s for the sS2CWL was reduced by more than 50% as compared with the respective S2CWL value in the PI0H and PI14H specimens.

BNC results for S2CWL and sS2CWL are displayed in **Fig. 7** and the BNC results for CCML are displayed in **Fig. 8**. The curves are averages of all the curves in a given group. In contrast to the more than 50% decrease in E_s for the sS2CWL as compared with the corresponding S2CWL in **Fig. 6**, the values of H actually increase slightly for the sS2CWL across the entire span of indentation strain rates shown in **Fig. 7**. For the S2CWL, specimens C and PI14 have the lowest values of H, and pMDI14H has the highest values of H. In the CCML, specimens C, PI14, PI0H have the lowest values of H and the values increase in specimens CH, PI14H, and specimen pMDI14H has the highest values. The shapes of the

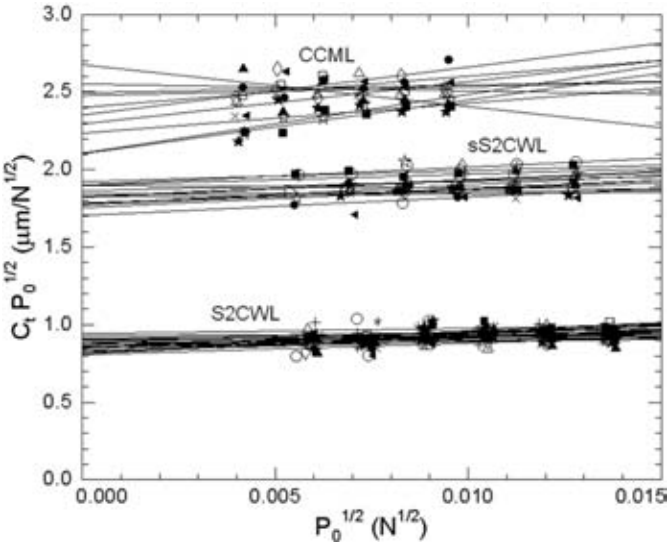

Figure 5. ~ *Stone, Yoder, and Sproul (SYS) correlations (Eq. [1]) of indents placed in specimen PI0H.*

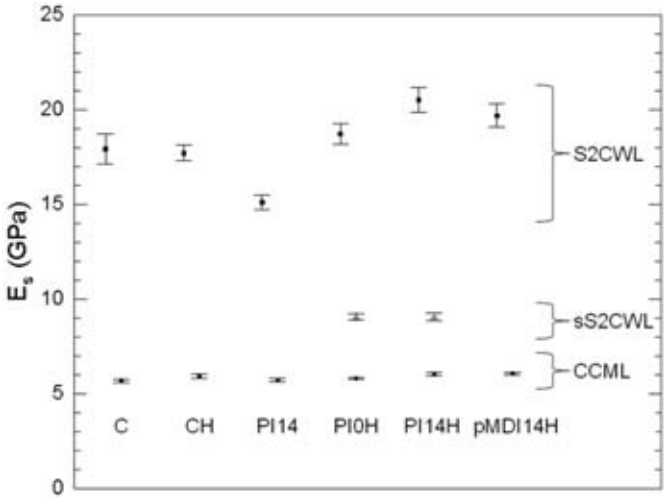

Figure 6. ~ *Elastic modulus, E_s, of indents placed in CCML, sS2CWL, and S2CWL. Error bars are standard error.*

Table 2. ~ *Number of indents and the average values of J_0 and C_m+C_s placed in the S2CWL, sS2CWL, and CCML of each specimen. Uncertainties are the standard error.*[a]

Specimen ID	n[b]			$J_0^{1/2}$			$C_m + C_s$		
	S2CWL	sS2CWL	CCML	S2CWL	sS2CWL	CCML	S2CWL	sS2CWL	CCML
				----------(µm/N$^{1/2}$)----------			----------(µm/N)----------		
C	21	–	10	0.88 ± 0.01	–	2.57 ± 0.06	6.8 ± 1.0	–	14.9 ± 6.4
CH	23	–	9	0.89 ± 0.01	–	2.38 ± 0.05	5.2 ± 0.7	–	30.2 ± 6.8
PI0H	24	14	10	0.87 ± 0.01	1.83 ± 0.02	2.37 ± 0.05	6.2 ± 0.7	7.9 ± 1.2	14.9 ± 6.4
PI14H	20	22	10	0.82 ± 0.01	1.70 ± 0.02	2.37 ± 0.05	7.5 ± 0.7	5.6 ± 1.1	30.0 ± 8.3
PI14	24	–	10	0.95 ± 0.01	–	2.69 ± 0.04	5.6 ± 0.5	–	-0.2 ± 5.1
pMDI14H	32	–	10	0.88 ± 0.01	–	2.24 ± 0.05	4.3 ± 0.9	–	32.0 ± 5.0

[a]Standard error calculated as standard deviation divided by the square root of number of indents (n).

[b]Number of indents analyzed. Indents observed to overlap a heterogeneity were discarded.

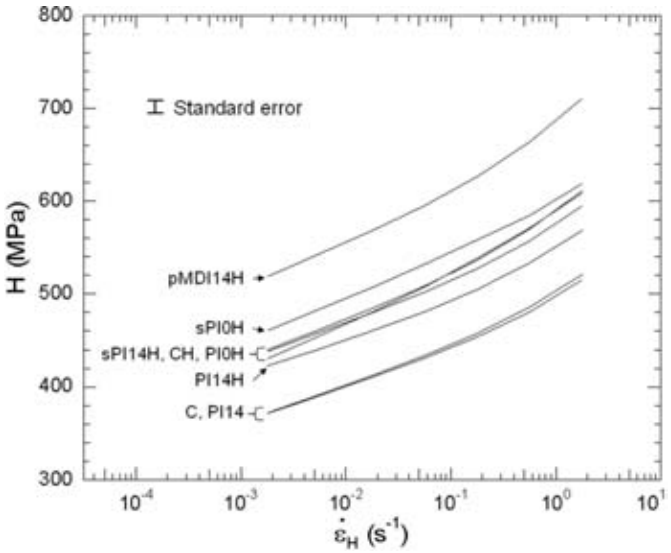

Figure 7. ~ *Broadband nanoindentation creep (BNC) data for indents placed in S2CWL and sS2CWL. The sS2CWL data are indicated with an "s" before the specimen name. Each curve is the average of the indents in the indicated group. Standard error was found to be independent of strain rate and consistent between each average curve.*

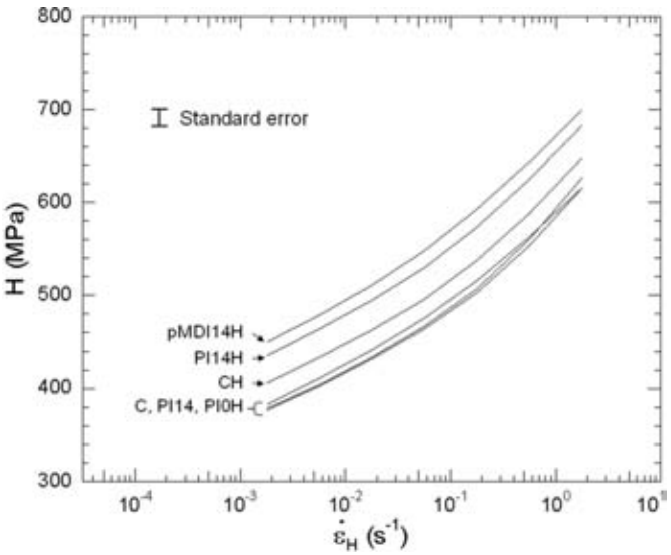

Figure 8. ~ *Broadband nano-indentation creep (BNC) data for indents placed in CCML. Each curve is the average of the indents in the indicated group. Standard error was found to be independent of strain rate and consistent between each average curve.*

BNC curves only change slightly between the treatments within the CCML and S2CWL.

Improved Understanding of Molecular-Scale Interactions between pMDI and Wood

As previously mentioned, our approach to gain an improved understanding of the pMDI-wood interactions was to react wood with phenyl isocyanate to create model B4 and compare the cell wall properties obtained using nano-indentation to those of pMDI-reacted wood. Ideally, this comparison would be carried out under identical reaction conditions, like between specimens PI14H and pMDI14H. However, results from Part 1 and here show specimen PI14H is not model B4. In Part 1, carbamate formation was observed from the 2D solution NMR spectra and here in Part 2 we observed the formation of the sS2CWL, similar to specimen PI0H, which was expected to form carbamates. Specimen PI14 was the only one likely with a model B4 interaction. However, specimens PI14 and pMDI14H were reacted at different temperatures. To take this into account, we will compare specimen PI14 to the room temperature control, and specimen pMDI14H to the heated control, specimen CH.

The S2CWL E_s (**Fig. 6**) of specimen PI14 is lower than that of specimen C and the S2CWL E_s of specimen pMDI14H is higher than that of specimen CH. The decrease in S2CWL E_s in specimen PI14 is consistent with a bulking effect and the increase in specimen pMDI14H suggests that a reinforcing phase is being added to the S2CWL. For the CCML E_s, the values did not change for specimens PI14 or pMDI14H compared with their respective controls. The S2CWL BNC data (**Fig. 7**) shows the largest differences between specimen PI14 and pMDI14H. Compared with their respective controls, H of PI14 does not change, and pMDI14H increases substantially in H. This again suggests that pMDI is forming a reinforcing phase in the S2CWL of specimen pMDI14H. The same trends are observed in the CCML BNC results (**Fig. 8**). These observed differences between specimens PI14 and pMDI14H suggest that the molecular-scale interactions of the infiltrated chemicals are different and the increases in E_s and H for specimen pMDI14H indicate that pMDI infiltrating the cell walls could be creating a reinforcing IPN phase (model B5).

Further discussion of the nano-indentation results and formation of the sS2CWL fall outside the scope of this proceeding, but will be the subject of future papers.

Conclusions

Nano-indentation of the cell walls modified with pMDI revealed an increase in E_s and H. These results suggest infiltrated pMDI polymerized in situ, creating an IPN of polyurea within the cell walls that serves as reinforcement. This work provides further insight into the mechanisms responsible for the durability of pMDI-wood bondlines. It supports the suggestion put forth by Frazier that IPNs form at the interphase of adhesives and wood (Frazier 2002). It is conceivable that the IPNs anchor themselves in the bulk adhesive and contribute to mechanisms transferring mechanical stress across the bondline. In addition, an IPN may alter the hygroscopic properties of wood and possibly reduce the swelling of wood in the presence of water.

Literature Cited

Elmustafa, A.A., S. Kose, and D.S. Stone. 2007. The strain-rate sensitivity of the hardness in indentation creep. J. Mater. Res. 22(4):926–936.

Frazier, C.E. 2002.The interphase in bio-based composites: What is it, what should it be? *In* 6th Pacific Rim Bio-Based Composites Symposium, Vol. 1. Portland, OR.

Frazier, C.E. 2003. Isocyanate wood binders. pp. 681–694. *In* A. Pizzi and K.L. Mittal (eds.) Handbook of Adhesive Technology. 2nd ed. Marcel Dekker, New York.

Gindl, W., and H.S. Gupta. 2002. Cell-wall hardness and Young's modulus of melamine-modified spruce wood by nano-indentation. Compos. Part A-Appl. S. 33(8):1141–1145.

Gindl, W., T. Schoberl, and G. Jeronimidis. 2004a. The interphase in phenol-formaldehyde and polymeric methylene di-phenyl-di-isocyanate glue lines in wood. Int. J. Adhes. Adhes. 24(4):279–286.

Gindl, W., T. Schoberl, and G. Jeronimidis. 2004b. Erratum: The interphase in phenol-formaldehyde (PF) and polymeric methylene di-phenyl-di-isocyanate (pMDI) glue lines in wood. Int. J. Adhes. Adhes. 24(6):535–535.

Jakes, J.E., C.R. Frihart, J.F. Beecher, R.J. Moon, and D.S. Stone. 2008. Experimental method to account for structural compliance in nano-indentation measurements. J. Mater. Res. 23(4):1113–1127.

Jakes, J.E., C.R. Frihart, J.F. Beecher, R.J. Moon, P.J. Resto, Z.H. Melgarejo, O.M. Surez, H. Baumgart, A.A. Elmustafa, and D.S. Stone. 2009. Nanoindentation near the edge. J. Mater. Res. 24(3):1016–1031.

Joslin, D.L., and W.C. Oliver. 1990. New method for analyzing data from continuos depth-sensing microindentation tests. J. Mater. Res. 5(1):123–126.

Konnerth, J., and W. Gindl. 2006. Mechanical characterisation of wood-adhesive interphase cell walls by nanoindentation. Holzforschung 60(4):429–433.

Konnerth, J., and W. Gindl. 2008. Observation of the influence of temperature on the mechanical properties of wood adhesives by nanoindentation. Holzforschung 62(6):714–717.

Konnerth, J., A. Jager, J. Eberhardsteiner, U. Muller, and W. Gindl. 2006. Elastic properties of adhesive polymers. II. Polymer films and bond lines by means of nanoindentation. J. Appl. Polym. Sci. 102:1234–1239.

Norimoto, M. 2001. Chemical modification of wood. pp. 573–598. *In* D.N.-S. Hon and N. Shirashi (eds.) Wood and Cellulose Chemistry. 2nd edition. Marcel Dekker, New York.

Oliver, W.C., and G.M. Pharr. 1992. Improved technique for determining hardness and elastic modulus using load and displacement sensing indentation experiments. J. Mater. Res. 7(6):1564–1580.

Puthoff, J.B., J.E. Jakes, H. Cao, and D.S. Stone. 2009. Investigation of thermally activated deformation in amorphous PMMA and Zr-Cu-Al bulk metallic glasses with broadband nanoindentation creep. J. Mater. Res. 24(3):1279–1290.

Stone, D.S., and A.A. Elmustafa. 2008. Analysis of indentation creep. pp. 163-168. *In* Fundamentals of Nanoindentation and Nanotribology IV, 26–29 Nov. 2007, Warrendale, PA. Materials Research Society.

Stone, D.S., J.E. Jakes, J.B. Puthoff, and A.A. Elmustafa. 2010. Analysis of indentation creep. J. Mater. Res. 24(3):611–621.

Stone, D.S., and K.B. Yoder. 1994. Division of the hardness of molybdenum into rate-dependent and rate-independent components. J. Mater. Res. 9(10):2524–2533.

Stone, D.S., K.B. Yoder, and W.D. Sproul. 1991. Hardness and elastic modulus of TiN based on continuous indentation technique and new correlation. J. Vac. Sci. Technol. A. 9(4):2543–2547.

Wimmer, R., and B.N. Lucas. 1997. Comparing mechanical properties of secondary wall and cell corner middle lamella in spruce wood. Iawa J. 18(1):77–88.

Wimmer, R., B.N. Lucas, T.Y. Tsui, and W.C. Oliver. 1997. Longitudinal hardness and Young's modulus of spruce tracheid secondary walls using nanoindentation technique. Wood Sci. Technol. 31(2):131.

Winandy, J.E., and R.M. Rowell. 2005. Chemistry of Wood Strength. pp. 303–347. *In* R.M. Rowell (ed.) Handbook of Wood Chemistry and Wood Composites. CRC Press, Boca Raton, FL.

Yelle, D.J. 2009. A solution-state NMR approach to elucidating pMDI-wood bonding mechnisms in loblolly pine. pp. 1–169. *In* Forestry/Chemistry, University of Wisconsin-Madison. Madison, WI.

Yelle, D.J., J.E. Jakes, J. Ralph, and C.R. Frihart. 2010. Characterizing pMDI reactions with wood cell walls: 1. High-resolution solution-state NMR spectroscopy. pp. 338–342. *In* Wood Adhesives 2009 Proceedings, Lake Tahoe, NV.

Yelle, D.J., J. Ralph, and C.R. Frihart. 2008. Characterization of nonderivatized plant cell walls using high-resolution solution-state NMR spectroscopy. Magn. Reson. Chem. 46:508–517.

Wood Adhesives 2009 / edited by Charles R. Frihart, Chiristopher G. Hunt, and Robert J. Moon.
Madison, WI : Forest Products Society, c2010. 1 CD-ROM.
ISBN 978-1-892529-57-2. FPS Proceedings no. 7216-09.